AD717669

DEVELOPMENT OF NONDESTRUCTIVE TESTING TECHNIQUES FOR DETECTING STRESS IN FERROMAGNETIC MATERIALS

by

C. G. Gardner

G. A. Matzkanin

D. L. Davidson

PHASE II
FINAL REPORT
SwRI Project No. 15-2474

Prepared for
Naval Air Engineering Center
Philadelphia, Pennsylvania
Contract No. N00156-69-C-0856
Sponsored by Advanced Research Projects Agency
ARPA Order No. 1247, Amendment No.1, Program Code No. 9D10

15 September 1970

Reproduced by
NATIONAL TECHNICAL
INFORMATION SERVICE
Springfield, Va. 22151

FEB 8

SOUTHWEST RESEARCH INSTITUTE
SAN ANTONIO HOUSTON

SOUTHWEST RESEARCH INSTITUTE
Post Office Drawer 28510, 8500 Culebra Road
San Antonio, Texas 78228

DEVELOPMENT OF NONDESTRUCTIVE TESTING TECHNIQUES FOR DETECTING STRESS IN FERROMAGNETIC MATERIALS

by
C. G. Gardner
G. A. Matzkanin
D. L. Davidson

PHASE II
FINAL REPORT
SwRI Project No. 15-2474

DDC
RECEIVED
FEB 3 1971
C

Prepared for
Naval Air Engineering Center
Philadelphia, Pennsylvania
Contract No. N00156-69-C-0856
Sponsored by Advanced Research Projects Agency
ARPA Order No. 1247, Amendment No.1, Program Code No. 9D10

15 September 1970

Approved:

John R. Barton

John R. Barton, Director
Department of Instrumentation Research

TABLE OF CONTENTS

LIST OF ILLUSTRATIONS

LIST OF ILLUSTRATIONS (Cont'd)

LIST OF ILLUSTRATIONS (Cont'd)

1. INTRODUCTION

1.1 Background

It is well known that many of the characteristic magnetic properties of a ferromagnetic material are strikingly influenced by the state of mechanical stress of the specimen in question.[1] It is therefore natural to inquire whether the stress dependence of some conveniently measurable magnetic parameter of such a material might not be made the basis of a practical method of quantitatively determining its state of mechanical stress. Suggestions along this line have by no means been lacking, having been made at least as early as 1922.[2] Of the numerous subsequent efforts to reduce such suggestions to practice, the work of Foerster and Stambke[3] may be taken as representative. There are three major circumstances which render this objective difficult of attainment. First, there is the question of what parameter is to be measured, i.e., what feature or features of the initial magnetization curve or of the hysteresis loop are most sensitive to, or vary most conveniently with, the state of mechanical stress. Second, it proves quite difficult in practice to make an accurate absolute measurement of a magnetic parameter of a specimen of complex geometry. Finally, the present state of our knowledge of the relation between the measurable magnetic parameters of a material, on the one hand, and its detailed metallurgical characteristics, on the other, is not sufficiently developed to enable us easily and reliably to distinguish the effects of mechanical stress from, say, compositional or structural influences. Consequently, stress measurement by magnetic means is presently seldom undertaken, and then ordinarily only in a comparative sense and under conditions where other pertinent parameters can be assumed invariable. Nevertheless, in view of the technical importance of controlling both applied and residual stress in ferromagnetic materials (particularly high strength steels), and considering the present lack of satisfactory means of so doing, there is considerable incentive to try to overcome the difficulties associated with the magnetic approaches.

In 1964, Leep suggested that measurements of the magnetic Barkhausen effect might afford a useful alternative to the measurement of parameters associated with the technical hysteresis loop, and reported some tentative experimental attempts to measure stress by means of the Barkhausen effect.[4] The term "Barkhausen effect" (so called for its discoverer[5]) refers to abrupt irreversible changes in the state of magnetization of a specimen, during which the rate of change of magnetization (resolved in a reference direction) greatly exceeds the mean rate of change of the bulk magnetization of the specimen as a whole. (This definition must be appropriately extended; vide infra.) Such virtually discontinuous "jumps" in magnetization are now known to be due principally to abrupt irreversible movements of mobile boundaries separating small subregions (called domains) of a macroscopic specimen. Each such domain is at all times very nearly magnetically saturated; an unmagnetized macroscopic specimen comprises a great number of such

domains, the magnetization of which varies in direction in a more or less random way, with the result that the average bulk magnetization is zero. Barkhausen jumps are also associated with the nucleation and sudden growth of such domains. Such magnetization jumps may be induced by an externally applied field, by raising the temperature of the specimen, or by the application of a mechanical stress.

Work subsequent to that of Leep, reported by Donaldson and Pasley[6], confirmed the general stress dependence of the Barkhausen effect, and resulted in the realization of crude but practical instrumentation based upon this stress dependence.[7] The work of Leep and Pasley was largely intuitional and empirical; their instrumentation, while effective and free of certain of the inconveniences of preceding magnetic methods of stress measurement, is nevertheless limited by the fact that it is based on a phenomenon for which a satisfactory foundation at the level of first principles has not yet been laid. With this in mind, the present series of investigations was undertaken specifically to try to clarify experimentally the manner in which a mechanical stress influences the dynamics of magnetic domains (including especially Barkhausen jumps), and to do so in such a way that basic theories of the process can be critically tested.

Since its discovery in 1917, the Barkhausen effect has been extensively investigated, although systematic and rigorous quantitative results have frequently been lacking. No attempt is made in this report to cite all pertinent literature; a comprehensive critical review of the literature on the Barkhausen effect through 1965 has been presented by Stierstadt.[8]

1.2 Objective and Scope of the Present Investigation

The aim of the program reviewed here is to establish a sound and adequate physical basis for the exploitation of the stress dependence of the Barkhausen effect as a means of measuring applied and residual stresses in articles made from ferromagnetic materials. With this objective in view, we are currently pursuing two related lines of investigation. On the one hand, we are employing the Kerr magnetooptic effect to study the effect of an applied uniaxial stress upon both the statics and dynamics of magnetic domains in metallurgically simple specimens, principally single crystals and large grain polycrystalline specimens of silicon-iron. The Kerr effect affords a means of optically imaging the superficial domain structure and studying it either by means of still or motion picture photography, or by photometric techniques. On the other hand, we are also employing the more conventional approach wherein Barkhausen jumps are sensed indirectly through the influence of their associated magnetic field variations upon a nearby induction coil. These investigations have not yet been brought to a definitive stage; this report is therefore intended as an interim progress report covering the work performed in Phase II of the program. Related investigations have been and are being

conducted by various workers (principally in Europe), the most comprehensive research being that of Stierstadt and coworkers.[9]

1.3 Brief Summary of Accomplishments of Phase II

The major part of the effort of Phase II was devoted to perfecting the apparatus and experimental technique required to perform photometric and cinematographic studies of dynamical magnetic domain processes as revealed by the longitudinal Kerr magnetooptic effect. The technical problems encountered in this aspect of the work proved to be somewhat more difficult than originally anticipated, and a correspondingly greater portion of the total technical effort was expended in solving them. However, the expended effort did result in a satisfactory solution of the problems encountered, with the result that high quality still and (low speed) motion pictures of domains were obtained, analysis of which has already begun to clarify the fundamental role which the mechanical stress field plays in the Barkhausen effect. Moreover, the problems of instrumentation and techniques required for photometric studies of the Barkhausen effect were largely solved, and some preliminary results obtained. It is therefore anticipated that the various magnetooptic techniques will now rapidly yield the experimental results for which they have been developed.

In addition to the magnetooptic effort, progress was made in using the inductive coil approach to study the Barkhausen effect. In particular, cylindrical specimens of polycrystalline silicon-iron suitable for use in the (previously designed and fabricated) nonmagnetic uniaxial stress fixture were designed and fabricated. Further, a bias field solenoid capable of accommodating these specimens and their corresponding search coils, and capable of being used with the specimens while they are in the stress fixture, was designed and fabricated. The entire arrangement was given a preliminary test, and operational difficulties identified. Preparations were made for the incorporation of a multichannel pulse height analyzer into the data acquisition system. The pulse height analyzer was not available during Phase II, but is available at the present time and is scheduled for use early in Phase III of the program

Apart from the experimental work, further progress in establishing a theoretical framework adequate to account for our observations was made. Selected preliminary results of the work performed during Phases I and II of this program were presented in a short paper at the April 1970, meeting of the American Physical Society, held in Washington, D. C.[10]

1.4 Organization of Phase II Final Report

The remainder of this report comprises: (1) a brief summary of the theory of the magnetoelastic interaction; (2) a detailed report of the work

performed in Phase II using the Kerr magnetooptic effect for sensing magnetic domains and dynamical domain processes; (3) a detailed report of the work performed in Phase II using the inductive coil method of sensing Barkhausen jumps; and, (4) a summary of results and a survey of plans for the work to be performed in Phase III of the program.

2. THEORETICAL CONSIDERATIONS

2.1 Introductory Remarks

It is conventional to discuss the properties of ferromagnetic materials in terms of various parameters associated with the so-called technical initial magnetization curve and hysteresis loop characteristic of the material. Figure 1 shows such a graph in schematic form, together with the definition of the customary parameters. The smooth appearance of such graphs is due solely to the properties of the instrumentation used to determine them. The implication of the discovery of the Barkhausen effect is that if variations in the bulk magnetization, M, are sufficiently well resolved, the corresponding graph would have the characteristic appearance depicted in Figure 2. If an electronic signal proportional to the time rate of change of magnetic induction of a coil inductively coupled to a specimen whose magnetization is varying periodically at a small but finite frequency, f_0, is Fourier analyzed the corresponding power spectral density would be expected to have the characteristic features illustrated in Figure 3. The general features of this figure have indeed been verified.[11] These remarks suffice to make it clear that to account theoretically for observed features of the Barkhausen effect, one requires nothing less than a complete theory of the magnetization curve. While impressive progress toward such a theory has been made, such a complete, validated theory does not in fact exist at present. The ensuing precis of theory is necessarily restricted in scope to selected aspects which serve to place in context the experimental results subsequently discussed.

2.2 Ferromagnetic Anisotropy and Magnetoelastic Effects

The modern theory of ferromagnetism supposes that with each (magnetically active) crystalline lattice site there is associated an atomic magnetic dipole moment arising conjointly from the intrinsic spin and orbital motion of electrons. Through the agency of a purely quantum mechanical exchange interaction, these atomic moments are strongly coupled to one another, the result being that at temperatures below a characteristic value (the Curie temperature), the equilibrium state of the system is an ordered arrangement of these moments in which the net magnetic moment of the system is nonvanishing. Further, through the agency of interaction between the spin and orbital motion of each electron, the energy of the ordered spin system is dependent upon the orientation of its net moment with respect to the crystalline lattice itself, i.e., the energy of the spin system is anisotropic. In general, the magnetic anisotrophy energy is a function of the lattice strain, with the consequence that the lattice spontaneously deforms (with respect to a theoretical state in which the magnetic interaction among atomic moments is switched off), the equilibrium strain being determined by the conditions that the sum of the magnetic anisotropy energy and the elastic energy of the lattice be minimal. Such deformation is termed spontaneous magnetostriction.

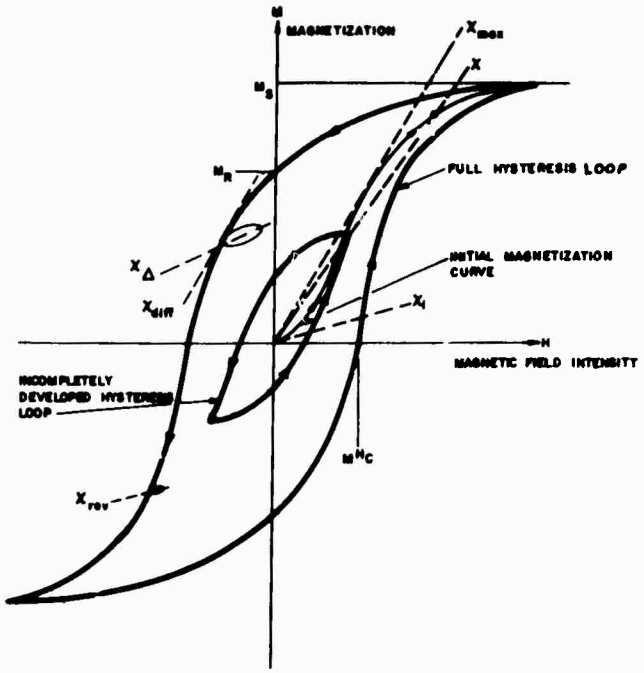

INITIAL SUSCEPTIBILITY $X = \left(\frac{dM}{dH}\right)_{M=H=0}$

"TOTAL" SUSCEPTIBILITY $X = \frac{M}{H}$ (WITH RESPECT TO INITAL CURVE)

MAXIMUM SUSCEPTIBILITY $X_{max} = \left(\frac{M}{H}\right)_{max}$ (WITH RESPECT TO INITIAL CURVE)

INCREMENTAL SUSCEPTIBILITY $X_\Delta = \left(\frac{\Delta M}{\Delta H}\right)_{H_0}$

"REVERSIBLE" SUSCEPTIBILITY $X_{rev} = \lim_{\Delta H \to 0} X_\Delta$

DIFFERENTIAL SUSCEPTIBILITY $X_{diff} = \left(\frac{dM}{dH}\right)_{H_0, I_0}$

SATURATION MAGNETIZATION M_S

REMANENT MAGNETIZATION M_R

(MAGNETIZATION) COERCIVE "FORCE" $_MH_C$

Figure 1. Schematic diagram of the technical magnetization curve of a ferromagnetic material indicating the conventional parameters associated with the curve.

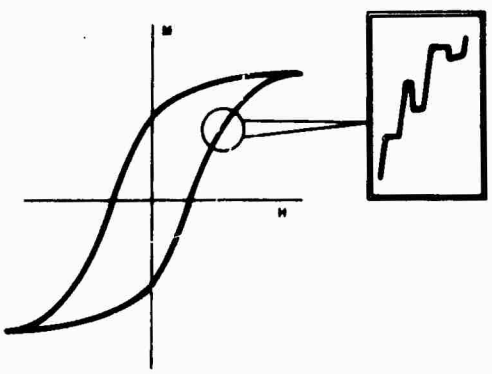

Figure 2. Schematic representation of the appearance of a portion of the magnetization curve as revealed by instrumentation of sufficiently great sensitivity and resolution.

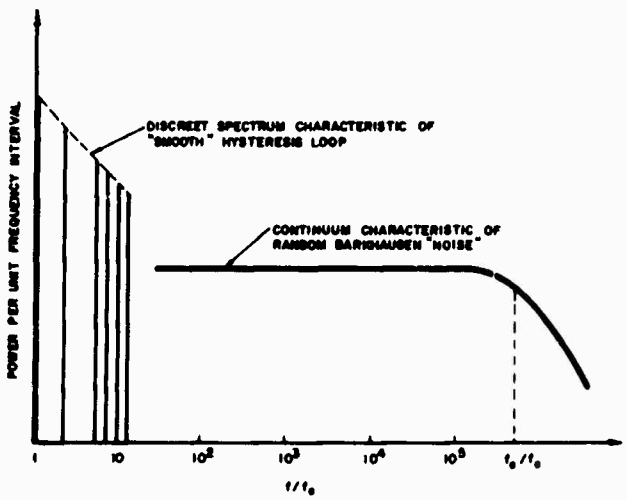

Figure 3. Schematic representation of the power spectral density of a signal V(t) produced in a wire coil inductively coupled to a ferromagnetic specimen undergoing cylic magnetization at frequency f_o. The frequency f_e at which loss of signal occurs is determined by eddy current damping in the specimen.

Following Kittel and Galt[12], one can write for the strain dependent magnetic anisotropy energy density the expression

$$E_k = E_k^0 + \sum_{i,j}\left(\frac{\partial E_k}{\partial e_{ij}}\right)_0 e_{ij} + \ldots . \qquad (1)$$

where the e_{ij} are the components of the symmetric strain tensor. The quantity E_k^0 is the magnetocrystalline anisotropy energy density for the unstrained lattice, and must therefore be consistent with the symmetry of the unstrained lattice. The coefficients $(\partial E_k/\partial e_{ij})_0$ are called the magnetoelastic coupling constants, and, taken collectively, must also be consistent with the symmetry of the unstrained lattice. The higher order terms are unimportant for iron. From these considerations, and specializing to the case of cubic symmetry (as appropriate to iron), it can be shown that E_k may be rewritten to sufficient accuracy in the form

$$E_k = K_1^0(a_1^2a_2^2 + a_2^2a_3^2 + a_3^2a_1^2) + B_1(a_1^2e_{11} + a_2^2e_{22} + a_3^2e_{33}) + 2B_2(a_1a_2e_{12} + a_2a_3e_{23} + a_3a_1e_{31}) \qquad (2)$$

where a_1, a_2, and a_3 are the direction cosines of the magnetization with respect to the cube axes.

Expressions relating the equilibrium strains of the lattice to elastic stiffness constants and the magnetoelastic coupling constants are obtained by minimizing the sum of E_k and the elastic energy of the lattice, the result being*

$$e_{ii}^0 = \frac{B_1[C_{12} + a_i^2(C_{11} + 2C_{12})]}{(C_{11} - C_{12})(C_{11} + 2C_{12})} ; \qquad (3a)$$

$$e_{ij}^0 = \frac{-B_2a_ia_j}{C_{44}} \quad (i \neq j) \qquad (3b)$$

Upon substitution of the foregoing strains into the right-hand side of Equation (2), one obtains the result

$$E_k = \left[K_1^0 + \left(\frac{2B_1^2}{C_{11} - C_{12}} - \frac{B_2^2}{C_{44}}\right)\right](a_1^2a_2^2 + a_2^2a_3^2 + a_3^2a_1^2) + (\text{isotropic term})$$

*Results differing from Equations (3a) and (3b) by numerical constants are given by some authors[13] who define the elastic stiffness constants by a different convention.

Thus, apart from contributing an additive isotropic term (which is conventionally dropped), the effect of the spontaneous magnetostriction is to shift the value of the anisotropy constant. The resultant effective anisotropy constant is denoted by the symbol K_1, the measured value for which (in iron) is 47×10^{-4} erg/cm^3. (14)

The relative change in the distance between two lattice points, induced by a homogeneous strain field e_{ij}, may be shown to be

$$\frac{\delta \ell}{\ell} = \sum_{i,j} e_{ij}\beta_i\beta_j \tag{4}$$

where β_1, β_2, and β_3 are the direction cosines of the (directed) line along which $\delta\ell$ is measured. Hence, the spontaneous linear saturation magnetostriction is obtained by evaluating the right-hand side of Equation (4) using the strains given by Equations (3a) and (3b):

$$\frac{\delta \ell}{\ell} = \frac{-B_1}{C_{11} - C_{12}} (\alpha_1^2\beta_1^2 + \alpha_2^2\beta_2^2 + \alpha_3^2\beta_3^2) - \frac{B_2}{C_{44}} (\alpha_1\alpha_2\beta_1\beta_2 + \alpha_1\alpha_3\beta_1\beta_3 + \alpha_2\alpha_3\beta_2\beta_3) + \frac{2C_{12}B_1}{(C_{11} - C_{12})(C_{11} + 2C_{12})} \tag{5}$$

Inasmuch as there does not exist a method of switching the ferromagnetic interaction among atomic moments on and off*, Equation (5) cannot be employed in a direct manner. Since the value of the isotropic term on the right-hand side of Equation (5) is not susceptible to measurement, it is conventional to replace it by the (also isotropic) term $B_1/3(C_{11} - C_{12})$, and thence to define dimensionless magnetostrictive constants λ_{100} and λ_{111} by the relations

$$\lambda_{100} = -\frac{2}{3}\frac{B_1}{C_{11} - C_{12}} \tag{6a}$$

$$\lambda_{111} = -\frac{1}{3}\frac{B_2}{C_{44}} \tag{6b}$$

converting Equation (5) to the form

*It is possible to destroy the ordered magnetic state by heating the specimen above its Curie temperature. This, however, affects both the magnetoelastic coupling constants and the elastic stiffness constants, whose temperature dependence near the Curie points have not been independently established.

$$\left(\frac{\delta \ell}{\ell}\right)' = \frac{3}{2}\lambda_{100}(\alpha_1^2\beta_1^2 + \alpha_2^2\beta_2^2 + \alpha_3^2\beta_3^2 - \frac{1}{3})$$

$$+ 3\lambda_{111}(\alpha_1\alpha_2\beta_1\beta_2 + \alpha_1\alpha_3\beta_1\beta_3 + \alpha_2\alpha_3\beta_2\beta_3) \qquad (7)$$

Here, the prime signifies that $(\delta\ell/\ell)'$ is defined according to the stated convention. λ_{100} may be interpreted as the relative change in length of a cube edge as the magnetization is rotated from a direction parallel to that cube edge to the direction of the cube diagonal, the specimen being magnetically saturated. The analogous interpretation of λ_{111} is obvious. Experimental values of λ_{100} and λ_{111} for pure iron are[15]

$$\lambda_{100} = +20.7 \times 10^{-6}; \quad \lambda_{111} = -21.2 \times 10^{-6}$$

Thus, for iron

$$\lambda_{111} \cong -\lambda_{100}$$

Accepting the experimental values for C_{11}, C_{12}, and C_{44} given by Kimura and Ohno[16], B_1 and B_2 turn out to be

$$B_1 = -2.94 \times 10^{-7} \text{ erg/cm}^3; \quad B_2 = 7.06 \times 10^7 \text{ erg/cm}^3$$

It is of prime importance to determine the contribution to the total energy density produced by a uniform uniaxial stress T applied to a specimen. If γ_1, γ_2, and γ_3 represent the direction cosines of the stress, relative to the crystal axes, then the elements of the symmetric stress tensor are $P_{ik} = T\gamma_i\gamma_k$ (T being taken to be positive for tension). This stress distribution induces the strains

$$e_{ij} = TS_{44}\gamma_i\gamma_j (i \neq j); \quad e_{11} = T[S_{11}\gamma_1^2 + S_{12}(\gamma_2^2 + \gamma_3^2)], \text{ etc.}$$

where s_4, s_{12}, and s_{44} are the nonvanishing, independent elastic compliance constants for the cubic lattice. Thus, referring again to Equation (2), the stress-induced magnetoelastic energy density is seen to be

$$E_T = T[B_1S_{12} + B_1(S_{11} - S_{12})(\alpha_1^2\gamma_1^2 + \alpha_2^2\gamma_2^2 + \alpha_3^2\gamma_3^2)$$

$$+ B_2S_{44}(\alpha_1\alpha_2\gamma_1\gamma_2 + \alpha_2\alpha_3\gamma_2\gamma_3 + \alpha_3\alpha_1\gamma_3\gamma_1)] \qquad (8)$$

Discarding the isotropic term on the right-hand side of Equation (8); eliminating B_1 and B_2 in favor of λ_{100} and λ_{111}; and using the approximation $\lambda_{111} \cong -\lambda_{100}$, Equation (8) for the stress-induced magnetoelastic energy density becomes

$$E_T = -\frac{3}{2} T\lambda_{100}[(a_1^2\gamma_1^2 + a_2^2\gamma_2^2 + a_3^2\gamma_3^2) - 2(a_1a_2\gamma_1\gamma_2 + a_2a_3\gamma_2\gamma_3 + a_3a_1\gamma_3\gamma_1)] \quad (9)$$

For application to the analysis of specimens in which the magnetization M lies parallel to a [100] type surface, Equation (9) further simplifies; upon setting a_3 equal to zero, one obtains the result

$$E_T = -\frac{3}{2} T\lambda_{100}(a_1\gamma_1 - a_2\gamma_2)^2 \quad (10)$$

For stresses within the elastic range of iron, $|\frac{3}{2} T\lambda_{100}|$ is small compared to the anisotropy constant K_1; hence, M will always essentially lie along an easy axis regardless of the applied stress, but will prefer the axis closest to the direction of tension (or, conversely, the easy axis most nearly normal to the direction of compression). If the easy axis lying closest to the direction of stress is taken as the x-axis, and ψ is the angle between the two directions, then E_T takes on one of the two forms

$$E_T^{(1)} = -\frac{3}{2} T\lambda_{100} \cos^2\psi; \quad \vec{M} \text{ parallel to x-axis} \quad (11a)$$

$$E_T^{(2)} = -\frac{3}{2} T\lambda_{100} \sin^2\psi; \quad \vec{M} \text{ perpendicular to x-axis} \quad (11b)$$

2.3 Magnetostatic Contributions to the Total Energy of a Ferromagnetic Specimen

The interaction energy density E_H resulting from the application of an external magnetic field intensity $\vec{H}_a$ to magnetized body is given by

$$E_H = -\vec{M} \cdot \vec{H}_a \quad (12)$$

$\vec{M}$ being the magnetic dipole moment per unit volume. A magnetized body will in general itself produce a magnetic field; if the intensity of such a field is denoted by $\vec{H}_s$, the resultant magnetic self-energy density of the body E_s is given by

$$E_s = -\frac{1}{2}\vec{M} \cdot \vec{H}_s$$

The evaluation of E_s for bodies of general shape and with complex distributions of magnetization usually cannot be performed exactly, necessitating approximation or numerical approaches. Alternative (but equivalent) expressions for E_s in terms of distributions of fictitious magnetic poles are frequently used.

2.4 Domains and Bloch Walls

The self-field of a uniformly magnetized finite body is always such as to render its total self-energy positive. A nonuniform distribution of magnetization can be achieved only at the expense of raising the exchange energy and the anisotropy energy of the system. In bulk ferromagnetic materials, it is found that adjacent regions with differing directions of M occur, between which there exists a comparatively thin transition region termed a Bloch wall. Within the wall region, and along a normal to it, the direction of magnetization (or a certain component thereof) continuously rotates in successive planes until it rotates through 180°. If the entire magnetization is affected, the result is a complete reversal of the direction of magnetization in passing through the wall, and the total magnetization is parallel to the wall on both sides of and through the wall. In iron (as well as some other materials) it also happens that walls may form the plane of which is at 45° with respect to the direction of magnetization, with only the component of M parallel to the wall reversing its direction in passing through the wall, the normal component remaining unchanged. Thus, such a wall separates regions in which the respective directions of magnetizations are perpendicular; such walls are termed 90° Bloch walls. The theory of Bloch walls is well developed[17] but cannot be reviewed here even cursorily. For present purposes, it need only be stated that the energy per unit surface area of 180° walls turns out to be $2(AK_1)^{1/2}$ where A is the exchange energy density and K_1 is the magnetocrystalline anisotropy constant. For 3.85 percent Si Fe, this was the value:[18]

$$E_{\pi} \cong 1.4 \text{ erg/cm}^2$$

The surface energy density of 90° walls is presumably one-half this value:

$$\frac{E_{\pi}}{2} = 0.7 \text{ erg/cm}^2$$

Regions of a specimen bounded by Bloch walls, and within which the magnetization is essentially uniform, are called domains. A nominally "demagnetized" bulk specimen comprises a number of domains whose volumes and directions of magnetization vary in a more or less "random" fashion so that the net magnetic dipole moment of the specimen is minimal. The size, shape, and arrangement of domains in a bulk specimen depends upon the size and shape of the specimen, its crystallographic state, the magnitude and direction of any externally applied magnetic field, and, finally, the applied and/or residual stress field to which the specimen is subject.

2.5 Domain Wall Movement and Barkhausen Jumps

When an external magnetic field is applied in a quasistatic manner to an initially nominally demagnetized iron specimen, the initial magnetization

process consists primarily of the growth in volume of favorably oriented preexisting domains at the expense of less favorably oriented ones. This takes place mainly through the displacement of 180° Bloch walls. As the magnetization progresses, more complex processes begin to contribute; these include the movement of 90° Bloch walls, the nucleation of new walls, the mutual annihilation of pairs of walls, and the disappearance of walls swept to the surface of the specimen. As the state of magnetization of the specimen approaches technical saturation, the domain structure is simplified; mobile walls are essentially eliminated; any remaining walls are essentially fixed in their configuration. A further increase in magnetization is achieved mainly through the rotation of the magnetization against the internal anisotropy forces. Barkhausen jumps occur chiefly (but not exclusively) in association with the movement of 180° walls. The mobility of such walls is determined principally by the manner in which the total magnetostatic energy of the specimen varies with wall movement. This in turn depends upon the size and shape of the specimen, and its detailed metallurgical structure. Magnetocrystalline anisotropy and magnetoelastic effects plays a important role in governing the overall domain structure energetically accessible, but are thought to be less important than magnetostatic effects in determining the mobility of preexisting domain walls (excepting the case of specimens essentially free of voids or inclusions). In the simplest conceptual model, irreversible movements of domain walls are presumed to occur as a consequence of the total energy of the specimen being a nonmonotonic function of wall displacement, i.e., stable positions of a wall exist at energies above that corresponding to the nominally demagnetized state of the specimen. In approaching such a stable position, a wall must be moved over a potential barrier, at which point it "spontaneously" moves to the stable position (local energy minimum). In electrically conductive ferromagnetics, the kinetic energy of the spontaneously moving wall is dissipated through the induction of localized eddy currents. Such wall potential models are inadequate to describe irreversible processes which involve the nucleation and growth of complex configurations of closure domains as a moving primary wall intercepts imperfections such as voids or nonmagnetic inclusions.

The irreversible processes accompanying wall motion are intimately related to the defect structure of the region of the crystalline lattice through which the wall is moving. Voids, foreign matter inclusions, dislocations, clusters of point imperfections, and mechanical stresses may influence wall motion. Of these, the effect of voids and nonmagnetic inclusions are presently reasonably well understood. The effect of point imperfections and dislocations has received theoretical attention, but few predictions of existing theories have been experimentally tested in any crucial sense. The situation in regard to single crystals has recently been reviewed by Träuble.[19, 20]

Mechanical stresses affect domain wall dynamics in two senses. In the first place, the surface energy density of a wall depends upon the effective local magnetocrystalline anisotropy constant K_1, which is stress dependent.

Secondly, the creation of a preferred cubic axis by a nonisotropic stress tends to induce the movement of 90° walls so as to minimize the total magnetoelastic energy, i.e., so as to leave the magnetization along the axis of lowest energy. The case of polycrystalline materials is further complicated by the existence of grain boundaries and the effects of crystalline misalignment.

A theory of irreversible processes in ferromagnetic material adequate to account quantitatively for the detailed features of the Barkhausen effect does not yet exist. Such a theory must account for: (1) the distribution of both magnitude and direction of rapid irreversible magnetization changes $\Delta\vec{M}$; (2) the complete temporal course of the magnetization jumps; (3) the coupling between magnetization jumps. These must be explained in terms of the metallurgical characteristics of the specimen, its geometry, and its state of mechanical stress.

3. MAGNETIC DOMAIN STUDIES BY MEANS OF THE KERR MAGNETOOPTIC EFFECT

3.1 Experimental Method

Use of the longitudinal Kerr magnetooptic effect for the observation of magnetic domains was first described in 1954 by Fowler and Fryer.[21] Since that time, the technique has become relatively well developed and has been used extensively in recent years. In general, the Kerr magnetooptic effect refers to the influence of magnetization on a linearly polarized light beam reflected from the surface of a magnetic specimen. Three Kerr effects-polar, transverse, and longitudinal are distinguished, depending on the disposition of the magnetization relative to the plane of the reflecting surface and the plane of incidence of the light beam. The polar effect pertains to the case where the magnetization is normal to the reflecting surface. For the other two effects, the magnetization vector lies in the plane of the reflecting surface. The transverse effect depends on the magnetization component perpendicular to the plane of incidence and involves a variation in the component of light polarized in the plane of incidence. The longitudinal effect depends on the magnetization component parallel to the plane of incidence and gives rise to a small additional component (Kerr component) in the reflected beam, lying in the plane orthogonal to that of the normal reflectance component, as illustrated in Figure 4. Magnetization components lying in the surface but having arbitrary directions with respect to the plane of incidence will, in general, result in a combination of transverse and longitudinal effects; however, the transverse effect can be eliminated by polarizing the incident beam perpendicularly to the plane of incidence. This is the situation that prevailed in the experiments reported here.

As indicated in Figure 4, the Kerr component in the reflected beam is slightly shifted in phase relative to that of the normal reflectance component. Thus the reflected beam is elliptically polarized with the major axis of the polarization ellipse rotated through an angle θ_k with respect to the original polarization direction, the sense of rotation depending on the magnitude of the magnetization component parallel to the plane of incidence. Therefore, as illustrated in Figure 5, rays reflected from localized regions (magnetic domains) of oppositely directed magnetization have their polarization rotated in opposite senses. A polarization analyzer set to extinguish rays whose polarization has been rotated in one sense will transmit a small amount of light whose polarization has been rotated in the opposite sense. Thus, the image formed by the reflected beam will contain regions of differing brightness corresponding to the variation in magnetization direction among the domains. Since the amount of rotation depends upon the magnetization component parallel to the plane of incidence, it is possible in principle to distinguish between varying relative magnetization directions of less than 180°. In practice, however, this is somewhat difficult to accomplish because of the

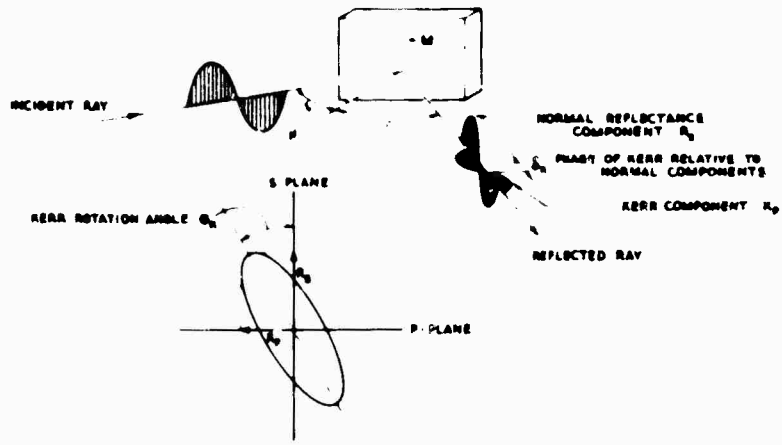

Figure 4. Longitudinal Kerr magnetooptic effect. The incident beam in polarized perpendicularly to the plane of incidence.

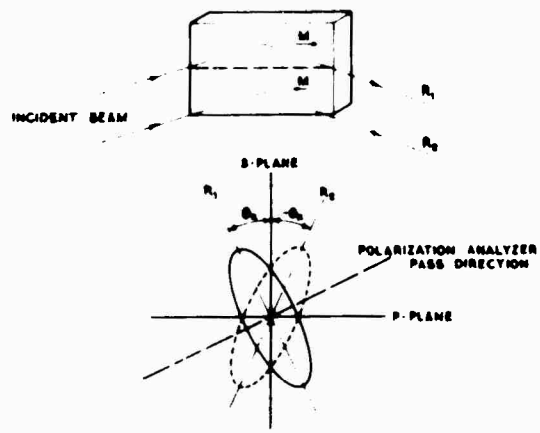

Figure 5. Observation of magnetic domains using nal Kerr magnetooptic effect. The polarization analyzer extinguishes ray R_1.

very small Kerr rotations involved (about 4 minutes of arc for saturated iron[22], and because of the nearly-crossed configuration of polarizers required to achieve optimum contrast. However, by making use of high-quality optical components and an intense, well-collimated laser light source, we have obtained sufficiently high image contrast to resolve relative magnetization directions of 90° as well as 180°.

The basic experimental arrangement used for the observation of magnetic domains by the longitudinal Kerr magnetooptic effect is illustrated schematically in Figure 6. Lasers used during the course of the experiments included a pulsed argon laser (4880Å and 5145Å) with an average power of 6 mW, and a continuous-wave 6-mW He-Ne laser (6328Å). The polarizer and analyzer were Glan-Thompson prisms, with a length of 14-mm and a 10-mm square aperture.

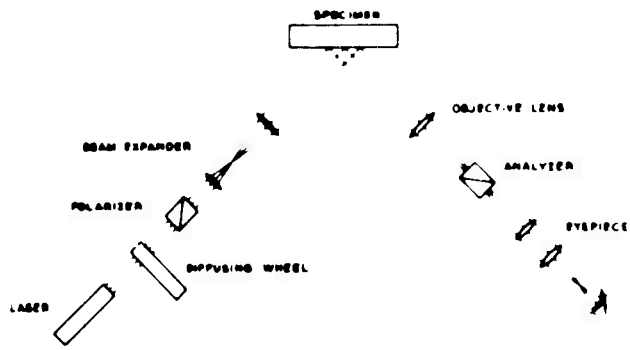

Figure 6. Schematic of longitudinal Kerr magnetooptic effect domain observation system. The analyzer is located at the focal point of the viewing objective in order to view the entire specimen surface.

3.2 Preliminary Exercises with Thin Films

Since the magnetooptic experiment involves reflected polarized light at a large angle of incidence (for our arrangement, the maximum Kerr rotation occurs at angles of incidence in the neighborhood of 60°) and extremely small light intensities at the final image plane, the specimen surface optical quality is of great importance. The requirement is for a very flat, scratch-free, highly reflective surface. Surface cold work strains must be removed so that the domain pattern representative of the bulk specimen is observed rather than the "maze" pattern associated with residual surface stresses.[23] In view of the (previously reported) difficulties encountered during Phase I in attempting to observe domains in bulk Fe-Si specimens, thin film specimens vacuum deposited on glass substrates were

used initially to permit the apparatus to be "tuned up." These materials generally meet the above requirements and provide good magnetooptic specimens. Specimens of permalloy (Fe-Ni) were obtained with thicknesses ranging from 300 Å to 1600 Å. After careful alignment and choice of optical components, domains were visually observed and photographed, as shown in Figure 7a.

Although the laser provides an intense, well collimated light beam nicely suited for this experiment, its coherence presents a problem in that any imperfections in the optical components, or in the specimen surface, generate diffraction and concomitant interference patterns which show up as "noise" in the recorded image, as illustrated by Figure 7a. However, experimentation showed that this problem could be largely overcome by introducing a rotating diffusing wheel into the incident beam. A transparent plastic disc thinly coated with a clear acrylic spray and rotated about its axis by means of a small motor proved suitable for this purpose. The diffusing disc randomly phase corrugates the laser beam wave front, and, if rotated at a speed fast with respect to the observation time, the interference patterns in the final image are effectively reduced by time averaging. The effect can be quite dramatic, as illustrated in Figure 7b, where domains at the edges can be readily observed.

Following the success in observing domains in thin films, various attempts were made to improve the experimental technique. Several methods of preparing the diffusing disc were tried; the disc was sprayed while stationary and while rotating with various amounts of clear acrylic spray. The acrylic spray was also smeared on by hand. It was found that too heavy a coating of acrylic spray would reduce the light intensity too much, whereas too little acrylic spray would not sufficiently reduce the noise. So it was necessary to strike a balance between the two extremes; spraying with the wheel rotating gave the most satisfactory results. It was found necessary to polarize the incident beam after diffusing to ensure that the beam impinging on the specimen would be adequately polarized. The effect of changing the angle of incidence was also investigated. A decrease in angle from 60° to 45° resulted in a slight (but noticeable) decrease in contrast, whereas lowering the angle to 15° brought about a relatively large decrease in contrast. For most of the experimental work, the angle of incidence was adjusted to approximately 60° to provide optimum contrast.

3.3 Initial Results on the Single Crystal

Figure 8 shows the results of an initial attempt to observe domains on the single crystal specimen of Fe-3% Si. As is evident, even with the diffusing disc, there is a substantial amount of "noise," resulting in a very grainy image. At this point in time, the specimen had been mechanically polished and electropolished using procedures described by other workers[24];

NOT REPRODUCIBLE

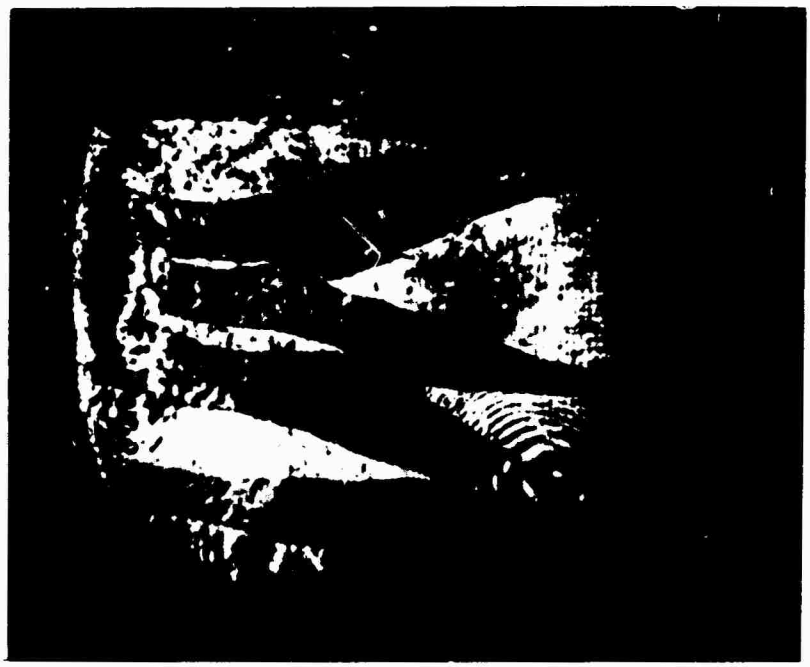

Figure 7a. Domains in a 77% Ni-23% Fe thin film 1600 Å thick and 1 cm in diameter. Angle of incidence 60°; no diffusing disc.

Figure 7b. Domains in a 77% Ni-23% Fe thin film 1600 Å thick and 1 cm in diameter. Angle of incidence 60°; with diffusing disc.

NOT REPRODUCIBLE

Figure 8. Magnetooptic observation of (100) surface of a 3% Si-Fe single crystal showing large amount of optical noise due to inadequately prepared surface.

although the surface appeared to the naked eye to be highly reflective, various imperfections (such as corrugation of the surface and a large number of small pits) could be observed under oblique lighting and microscopic examination. An attempt was made to overcome the noise problem by optical spatial filtering techniques.[25] Since the image noise resulting from surface imperfections is independent of the domain pattern, the procedure tried was to construct a Fourier amplitude filter of the noise with the specimen magnetically saturated (no domains). Insertion of the filter in the Fourier plane of the reflected beam should, in principle, mask out the "noise" part of the spatial frequency spectrum while allowing the domain image to come through. In practice, the procedure proved to be quite difficult and was abandoned after several unsuccessful attempts.

3.4 Specimen Preparation and Observation of Domains

It became clear that, in order to carry out the proposed experiments on the single crystal, drastic improvements would have to be made in the quality of the surface. After some discussion regarding surface preparation techniques and metallurgical consultation, it was decided to try mechanical polishing of the surface followed by a vacuum anneal to remove cold-working strains, omitting any electropolishing. It was found that polishing with alumina grit resulted in a flat surface substantially free of undulations and scratches, although small surface pits persisted. The surface quality was sufficiently improved, however, to enable observation of domains in the single crystal. Figure 9 shows the first photograph of the domains observed in the Fe-3% Si single crystal specimen. Efforts to improve the surface quality with longer polishing times using successively finer alumina grit were unsuccessful, the persistent pitting resulting in an unacceptable degradation of the magnetooptic image. After considerable effort and experimentation, it was found that polishing with diamond grit gave a very good, substantially

NOT REPRODUCIBLE

Figure 9. Magnetic domains observed magnetooptically on a (100) surface of a 3% Si-Fe single crystal after mechanical polishing with alumina and vacuum annealing. Width of striped domains is about 3 mm.

pit- and scratch-free surface which, after vacuum annealing, resulted in an unusually high-contrast domain image, as depicted in Figure 10.

An expanded optical field of view encompassing the entire specimen surface was obtained by expanding the incident beam and placing the analyzer prism immediately before the focal point of the objective lens. The contrast obtained is especially striking when account is taken of the fact that the surface has not been "bloomed" with a contrast-enhancing dielectric coating.[26] Such coatings have been used by other workers to improve the domain contrast (at the expense of image brightness) by causing a reduction in magnitude of the normal reflectance component of the reflected beam by means of destructive interference. Since our experiment involves stressing the specimen, it was thought that such dielectric coatings might result in inhomogeneous surface stresses, and therefore have not been used thus far. Due to a tendency for the highly polished, clean surface to rust when exposed to ambient conditions during the experiment, it may prove necessary to protectively coat the surface.

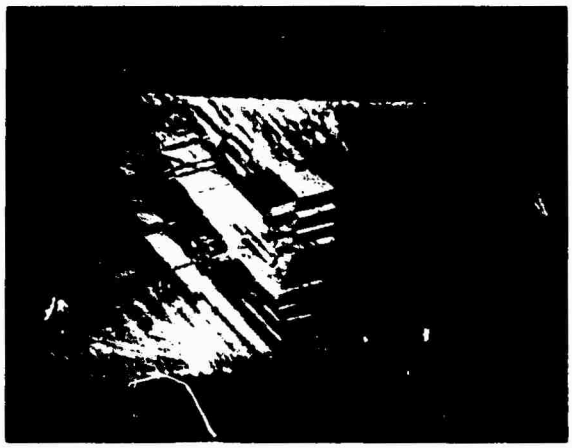

Figure 10. Magnetooptically observed domain patterns on a (100) surface of a 3% Si-Fe single crystal after mechanical polishing with one micron diamond and vacuum annealing. The entire 1 × 3-cm face of the specimen is observed.

The final specimen preparation procedure producing the best results is as follows: first, a mold with a cavity to accept the specimen was made of dental plastic. A ring of stainless steel tubing was embedded in the mold around the specimen cavity in order to minimize edge rounding during the polishing operation. The single crystal specimen was held within the cavity during polishing by a low melting temperature wax. After mounting, the specimen was faced on 600 grit SiC paper, then with 6-micron diamond on nylon cloth with methanol as a lubricant, and finally with 1-micron diamond on lint-free cotton with methanol as a lubricant. The surface produced was flat and substantially scratch- and pit-free, but with a heavily cold worked surface layer which prevented the observation of bulk domains. The crystal was then carefully cleaned in an ultrasonic agitator, placed in an alumina boat and annealed in a dynamic vacuum of better than 10^{-5} torr at 800°C. This temperature was chosen to be above the Curie temperature, below the $\alpha - \gamma$ transformation temperature and sufficiently high to ensure complete annealing. The specimen was heated to the annealing temperature over about a 4-hr period, held at 800°C for 2 hr and then allowed to cool to room temperature at the cooling rate of the closed furnace. The cool-down period was about 12 hr. When not in use, the specimen is stored in a dessicator because of the strong tendency for corrosion.

3.5 Static Photographic Studies of the Effect of Applied Magnetic Field and Mechanical Stress

The domain pattern displayed in Figure 10 is that of the demagnetized specimen, that is, the overall bulk magnetization is zero. During the course

of several months, the surface of the specimen was refinished several times according to the procedure outlined above, with the same general pattern of Figure 10 appearing on re-examination. Details differed from time to time, but the basic features remained the same.

In order to study the effects of an applied magnetic field and mechanical stress on the domain patterns, provisions were made for simultaneously changing the applied magnetic field and applying a uniaxial stress. A soft iron yoke C-electromagnet was constructed with pole tips machined to fit the specimen ends. The pole pieces are allowed to slide on the armature shaft providing a means of applying stress to the specimen while maintaining a low reluctance contact through the close fit of the pole pieces and armature. The armature coil consists of 2580 turns of No. 22 copper wire and provides an air gap field of approximately 900 Oe/amp. Pole piece adapters were constructed to connect the magnet pole pieces to the chucks of the nonmagnetic uniaxial stressing fixture constructed in Phase I. The arrangement was so designed that the stress would be uniformly applied parallel to a long edge of the rectangular specimen. Figure 11 is a photograph of the assembly showing the stressing fixture, the magnet, and the

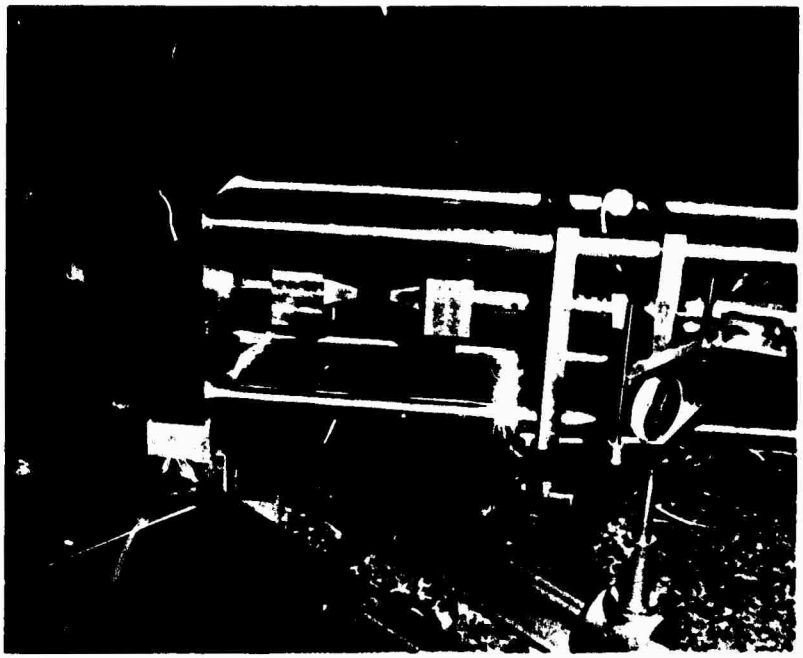

Figure 11. Electromagnet and specimen in stressing fixture.

specimen contained within the pole pieces. Figure 12 is a view of the entire experimental setup. At the present time, only application of compressive stress has been undertaken. The problems involved in gripping the specimen

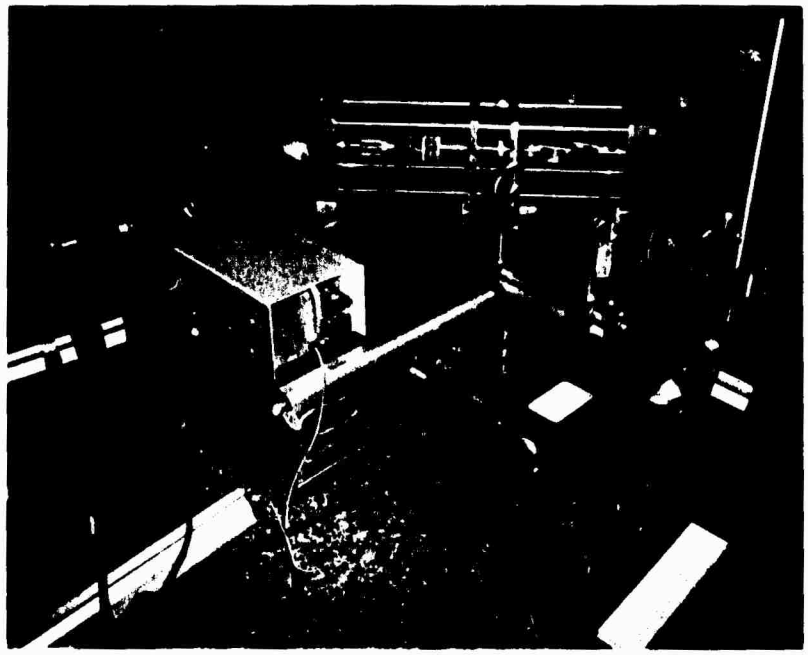

Figure 12. Overall view of longitudinal Kerr magnetooptic effect domain observation system.

during application of tensile stress so as not to cause damage have been reviewed and are expected to be solved during the next phase of the program.

Current is supplied to the electromagnet by a bipolar programmable power supply. A signal generator supplying a triangular waveform is used in conjunction with the power supply to vary smoothly and slowly the current through the magnet coil, and thus also to vary the magnetic field applied to the specimen.

Figure 13 shows schematically the specimen dimensions and orientation. The observed surface is nominally normal to a ⟨100⟩ direction, with the other magnetically "easy" directions lying in the surface. Figure 14a is a top view of the specimen surface. The surface "easy" directions are oriented with respect to the specimen axis at angles of 55° and 35°, respectively. The specimen axis is 10° away from a ⟨110⟩ type direction. In Figure 14b, the crystal axes are shown projected on a plane normal to the reflected beam; i. e., the plane on which the magnetooptic image is formed.

Figure 15 shows the overall domain pattern observed on the surface of the nominally demagnetized specimen. The largest domain widths are on the order of 3 mm, or about the same as the thickness of the specimen, suggesting that these domains extend through the thickness of the crystal. This assumption is supported by the observation of closely similar domain

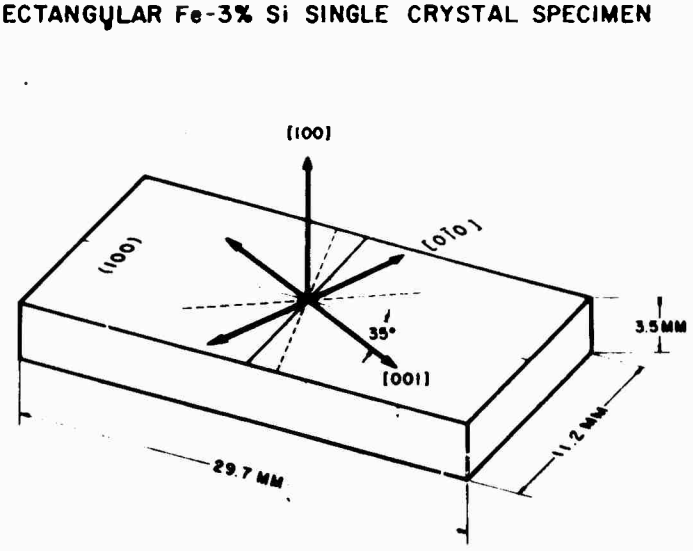

Figure 13. Dimensions and crystallographic orientation of rectangular silicon-iron single crystal used in magnetooptic studies of magnetic domains.

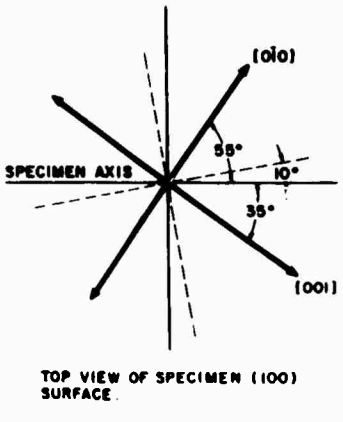

Figure 14a. Relative orientation of the crystalline axes and the specimen axis on the surface of the specimen.

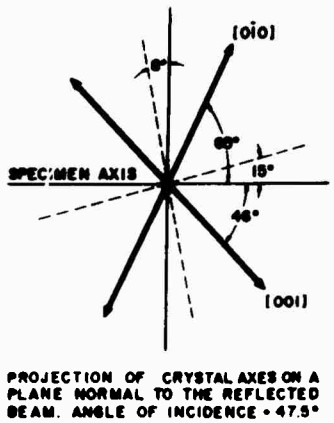

Figure 14b. Projection of the crystalline axes on the plane in which the magnetooptic image is formed, for an angle of incidence of 47.5°.

Figure 15. Demagnetized 3% Si-Fe single crystal domain pattern on a (100) surface. The domain magnetization directions are indicated by arrows. The entire specimen surface is viewed with the largest domain widths on the order of 3 mm.

patterns on the reverse face of the specimen. The appearance of "fir tree" domain patterns in this picture and in higher magnification Bitter pattern pictures indicate that the specimen surface is misoriented by about one degree with respect to a crystallographic (100) plane. The large V-shaped regions coincide with "easy" magnetization directions, whereas the walls most nearly parallel to the specimen axis are in a (100) direction. Because of the high anisotropy energy of Si-Fe, the magnetization is essentially confined to "easy" (100) directions, thus giving rise to 180° walls parallel to (100) directions, and 90° walls parallel to (110) directions. This interpretation is supported by a small but distinct contrast in image brightness which can be noted on careful inspection of the photographs. Although more evident in other higher-magnification photographs which we have made, these brightness variations can be seen in this picture in the "checkerboard" area. So instead of just "black" and "white," we also observe two distinct intermediate shades of gray. Analysis of the Kerr effect indicates that such contrast variations should be expected for the assigned magnetization directions. The four magnetization components parallel to the plane of incidence, to which the longitudinal Kerr effect is sensitive, differ in magnitude and direction, giving rise to the four domain shades observed here. The relative brightness variations predicted from analysis of the Kerr effect for the particular specimen orientation we have agree with the foregoing interpretation of the magnetization directions.

Figure 16 shows the effect of increasing the applied magnetic field along the specimen axis. The most favorably oriented domains have increased in size, primarily by movement of 180° walls. The lower mobility of the 90° walls parallel to the (110) direction is evident. One also notes the

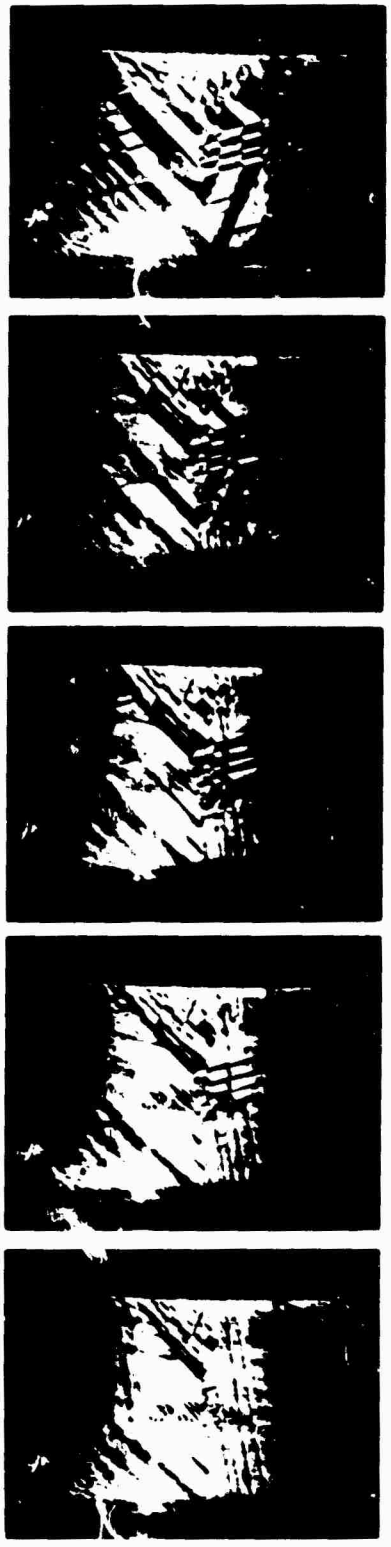

Figure 16. The effect on magnetic domains in a 3% Si-Fe single crystal caused by a magnetic field applied along the specimen axis. From top to bottom, the applied fields for successive frames are approximately: 0 Oe, 3 Oe, 6 Oe, 9 Oe, 12 Oe.

beginnings of stripes in the other (110) direction, and near saturation, the specimen is almost completely taken over by the stripes. Visual examination of the dynamic magnetization process and the contrast between these stripes suggest that these are domains separated by 90° walls. The inequality of the width of alternate domains is interpreted as being due to the fact that the "easy" (100) directions are not symmetrically oriented with respect to the specimen axis, and unequal width is therefore expected in order to minimize the net transverse magnetization. As the field is further increased toward saturation, the less favorably oriented domains (the narrow ones in Figure 16) shrink and finally disappear.

The effect of applying a compressive load to the specimen at zero applied field is shown in Figure 17. As can be seen, compressive stress induces the formation of domains in the easy direction farthest from the stress axis, i.e., at an angle of 55°. This behavior is theoretically expected for iron under compressive stress. Subsequent attempts to further document the effects of stress on the magnetization process in this specimen have indicated that the domain patterns are extremely sensitive to residual stresses (and probably to the metallurgical condition of the specimen) so that reproducible results are difficult to obtain. Work is currently in progress to better define the effects of metallurgical preparation on the domain patterns.

Also investigated briefly during the course of the work was a large-grain polycrystalline Fe-3% Si specimen. After surface preparation similar to the single crystal specimen, domain patterns were observed and photographed, as illustrated in Figure 18. Here, of course, the domains are very much smaller than in the single crystal and appear as light and dark irregular streaks. More detailed investigation of the polycrystalline domain patterns will be pursued at somewhat higher magnification in the next phase.

3.6 Dynamic Photographic Studies

At this point, attempts were made to record cinematographically dynamical domain processes, which is the ultimate objective of the magneto-optic effort. However, although domain dynamics were easily followed visually through the eyepiece, it became clear that the currently available light level and inherently high optical attenuation in the magnetooptic experiment (about 2×10^{-6} in our case), made high-speed, short-exposure-time cinematography impossible. As has been mentioned previously, long exposure times were generally needed; even with Polaroid 3000 speed film, exposure times of 10 sec were needed at magnifications of 3X. For film transport speeds of 10,000 frames per sec, which may be needed to resolve temporally the rapid Barkhausen jumps, an increase in source intensity of several orders of magnitude over that presently available to us is required. Some investigators have recently employed stroboscopic flashlamps for studies of domain dynamics using the Kerr effect, but have not reported the resolution of

Figure 17. The effect on magnetic domains in a 3% Si-Fe single crystal caused by a compressive stress applied along the specimen axis. From top to bottom, the applied stresses for successive frames are approximately: 0.6 kg/mm^2, 1.22 kg/mm^2, 1.84 kg/mm^2.

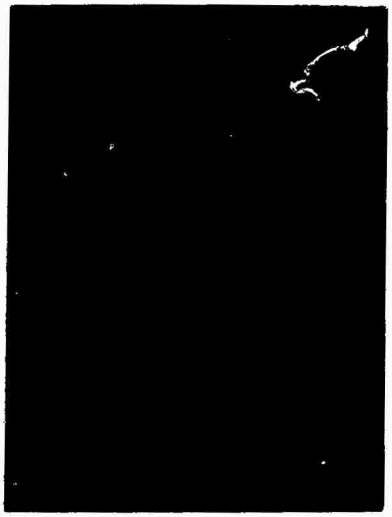

Figure 18. Magnetic domains observed magnetooptically in a large grain polycrystalline silicon-iron specimen. The domains are visible as light and dark streaks.

Barkhausen processes.[27, 28, 29] Recently available high-power stroboscopic pulsed lasers may provide a satisfactory solution to the source intensity problem, and are being evaluated for this application.

By reducing the image size to a 16-mm format and using the fastest speed movie film available (high-speed recording film developed to an exposure index of 5000) it was possible to make low-speed (16 frames per sec) movies of moving domains. Although the framing speed was too slow to resolve the irreversible magnetization processes, the results served to establish the capabilities of the technique and aided in the interpretation of the static results. It is anticipated that, in the near future, a light source with sufficient intensity for high-speed cinematography will become available.

3.7 Dynamic Photometric Studies of Barkhausen Jumps

An alternate method for studying dynamic domain processes via the Kerr effect is to make use of photometric sensors. As the magnetization of the specimen is reversed, the total intensity of the light beam emerging from the polarization analyzer will depend directly upon the net fractional magnetization reversal that has occurred in the portion of the specimen being illuminated by the beam. Thus, the instantaneous bulk magnetization state of the specimen can be inferred from a measurement of the beam intensity. In this method, the reflected light beam is focused and allowed to impinge upon the cathode of a photomultiplier tube placed immediately after the analyzer prism, the output of the photomultiplier being connected to an oscilloscope. As the magnetic field applied to the specimen is slowly changed, corresponding magnetization changes are manifested as vertical deflections of the oscilloscope trace. Figure 19a shows a hysteresis loop of a permalloy thin film specimen recorded this way, and Figure 19b is an expanded sweep of a single magnetization reversal of the same thin film, clearly showing Barkhausen jumps. By making a number of such photographs and measuring the sizes of the steps in the oscilloscope trace, it is possible to obtain a statistical distribution of Barkhausen jump sizes. This was done for a 1600-Å thick permalloy thin film. The results of such measurements are shown in Figure 20. Here the integral jump number (which is the number of observed jumps equal to or greater than a given size) is plotted as a function of the jump size. The jump size is taken to be the ratio of the individual change in magnetization to the total change in magnetization between saturation points. The results are found to be approximately fitted by the empirical relation[30]

$$\frac{N}{N_0} = A \exp[-K(M/M_T)]$$

NOT REPRODUCIBLE

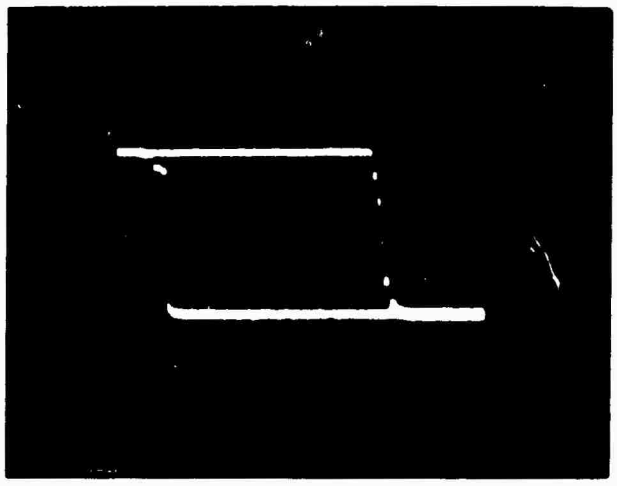

Figure 19a. Magnetooptically determined hysteresis loop of a 77° Ni-23% Fe permalloy thin film (1600 Å thick), obtained photometrically. The vertical axis is proportional to the magnetization of the specimen; the horizontal axis is proportional to the magnetic field applied to the specimen (frequency=0.09 Hz). Note the evidence of discontinuous changes (Barkhausen jumps) in the magnetization.

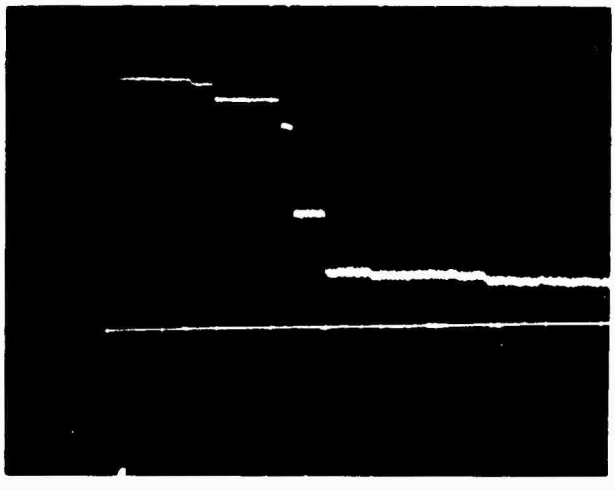

Figure 19b. Magnetooptically and photometrically determined Barkhausen jumps in one complete reversal of magnetization of the permalloy thin film. Note the variation in magnitude of the jumps.

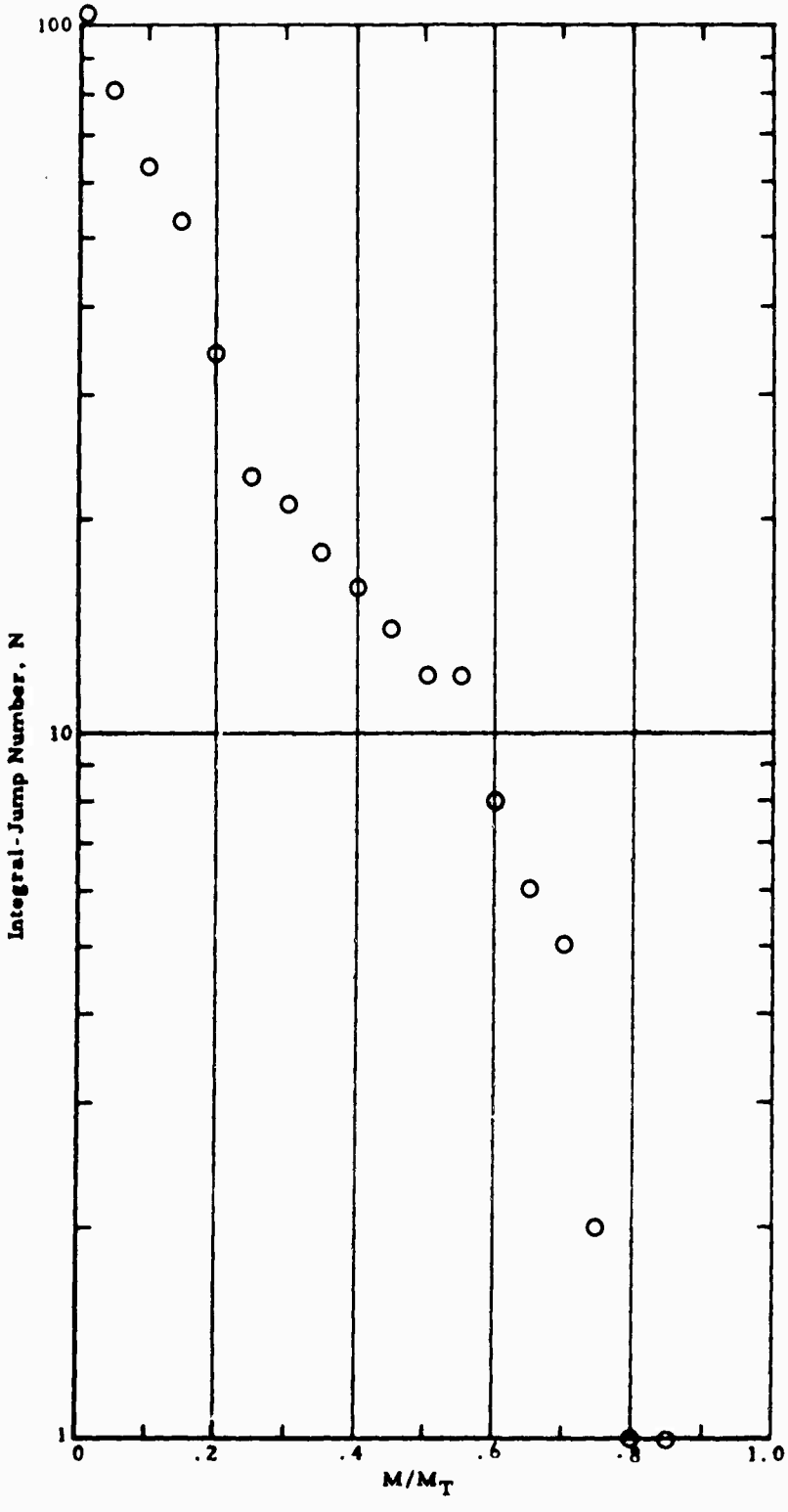

Figure 20. Integral size distribution of Barkhausen jumps in a 77% Ni-23% Fe permalloy thin film 1600 Å thick. Jump sizes were measured photometrically, using the Kerr magnetooptic effect.

where

A and K are constants characteristic of the film

N = number of jumps of size M or greater

N_0 = total number of jumps (of all sizes)

M = magnetization change in a given Barkhausen jump

M_T = total saturation magnetization of the specimen region in which magnetization changes are observed

The situation in the case of the Si-Fe single crystal is complicated by the complexity of the domain structure and the smallness of jump sizes in comparison to that of the thin film. Figure 21a shows a typical magnetization reversal in the single crystal as observed photometrically. As is evident, the discontinuous magnetization changes are not so well-defined as in the case of the thin film; however, definite discontinuities in the magnetization change can be observed. Rapid changes in the magnetization can be more readily discerned by using a high-pass filter at the photomultiplier output, providing AC coupling to the oscilloscope. A magnetization reversal observed in this way is shown in Figure 21b where the spikes correspond to rapid magnetization changes. The signal-to-noise ratio is rather poor due to the small amplitude of the jumps; however, this problem should be ameliorated by resorting to differential amplifier techniques. We believe the potential of this approach to be substantial, and are currently refining it for further application to the single crystal and other specimens.

NOT REPRODUCIBLE

Figure 21a. Magnetooptically and photometrically detected magnetization reversal in a small region of a 3% Si-Fe single crystal. The ordinate is proportional to the net surface magnetization; the abscissa is proportional to the magnetic field applied to the specimen. Note the discontinuous changes in magnetization.

Figure 21b. Oscillogram showing the time rate of change of surface magnetization of the 3% Si-Fe single crystal specimen as the state of magnetization is slowly reversed. Note the Barkhausen pulses. (Low frequencies have been blocked.)

4. INDUCTIVE COIL BARKHAUSEN EXPERIMENTS

Apparatus was assembled for conventional specimen-encircling inductive coil Barkhausen experiments, and investigations of polycrystalline Fe-Si specimens were initiated. The specimens are cylinders 3-in. long and 1/4 in. in diameter with a raised shoulder on each end to provide a means of gripping the specimen for the application of stress. Adapters were constructed of nonmagnetic materials and used to connect the specimen to the chucks of the nonmagnetic stressing fixture. The overall design allows the application of both tensile and compressive stress and easy changeover of specimens. A specimen with the adapters attached is shown in Figure 22. An available solenoid suitable for the magnetizing field was modified to provide a large enough bore for the specimen and adapters. The solenoid comprises 8100 turns of No. 18 copper wire, and provides a field of 380 Oe/amp at the center of the bore. The programmable power supply and signal generator used in the magnetooptic work provides the magnetizing current.

Figure 22. Cylindrical polycrystalline silicon-iron specimen and adapters for application of stress.

A variety of search coils for the detection of Barkhausen signals have been fabricated. Some were wound on phenolic tubes containing the specimen and others were wound directly on the specimen to provide closer inductive coupling.

The signals induced in the search coil were amplified with a Tektronix Type 1A7A high-gain differential plug-in amplifier and displayed on an oscilloscope. Figure 23a is a photograph of the Barkhausen noise induced in a 200-turn coil wound directly on the specimen during a complete traversal of the hysteresis loop. Figure 23b is an expanded trace of one of the noise bursts.

Figure 23a. Barkhausen noise induced in a specimen encircling 200 turn search coil during a traversal of the hysteresis loop. The specimen is a 1/4-in.-diameter rod of polycrystalline, 3% Si-Fe. The vertical sensitivity is 50 μv/cm and the horizontal time scale is about 5 sec/cm.

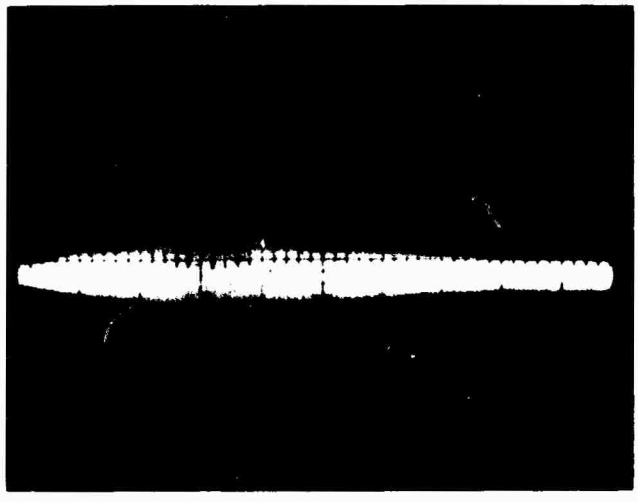

Figure 23b. Expended time scale of a single burst of Barkhausen noise in a 3% Si-Fe polycrystalline specimen 1/4 in. in diameter. The vertical sensitivity is 100 μv/cm and the horizontal time scale is 0.2 sec/cm.

A major difficulty encountered was the presence of strong interference from power lines, lighting fixtures, etc. Although use of the differential input to the plug-in amplifier greatly ameliorated this situation, it became apparent that a separate preamplifier was in order. Since the desired signals are in the microvolt range, and have spectral content into the MHz range[31], a low-noise, wide-band preamplifier is required. The preamplifiers presently available are marginal in terms of their noise figure, and possible alternatives are being investigated.

Inductive coil Barkhausen jump detection and characterization will be intensively pursued in Phase III of this program.

5. CONCLUSIONS

5.1 Summary of Results

The major effort expended during Phase II was devoted to establishing a capability for the study of magnetization processes by the longitudinal Kerr magnetooptic effect. Mastery of the experimental technique absorbed more time than originally anticipated, but the final results, in terms of a better understanding of the role of magnetoelastic interactions in stress measurements in magnetic materials, are deemed to be worth the effort.

In addition to the magnetooptic work, inductive coil Barkhausen experiments were initiated on various polycrystalline specimens of silicon-iron and steel. Although results at this time are sparse, instrumentation requirements have been clarified, and a variety of experiments have been designed for execution during the Phase III.

The results realized during Phase II can be summarized as follows:

(1) A theoretical framework was developed to aid in the analysis of experimental data on the effects of stress on domain structures and magnetization processes. An attempt was made to clarify and unify existing theoretical approaches in a way adapted to the particular circumstance prevailing in the work reported herein.

(2) A magnetooptic facility was constructed for the observation and study of magnetic domains, and the experimental method mastered.

(3) Techniques were developed for the preparation of surfaces on bulk silicon-iron suitable for magnetooptical observation of magnetic domains with good contrast.

(4) Fixturing was designed and constructed for the simultaneous application of magnetic field and mechanical stress to a rectangular, single-crystal specimen. Use was made of the nonmagnetic stressing machine constructed during Phase I.

(5) Static photographic records were made of the effect of applied magnetic field and mechanical stress on the domain patterns on a (100) surface of a 3% Si-Fe single crystal specimen. In general, the gross features of the patterns can be explained in terms of existing theories of magnetization. By using an expanded laser beam, domain patterns were observed over the entire 1 cm × 3 cm (100) surface of the specimen and 90° Bloch walls as well as 180° walls were clearly resolved. Application of compressive

stress forced the magnetization to align in domains in the magnetically "easy" direction farthest from the stress axis. Magnetization of the specimen then proceeds largely by domain nucleation affording a possible explanation for the empirical observation of decreased Barkhausen activity under compressive loading, as reported in the Phase I Final Report.

(6) Domain dynamics were studied cinematographically. Although the available laser light source was not of sufficient intensity for high-speed studies, low-speed movies (16 frames per sec) were successfully made of the influence of compressive stress on the magnetization process.

(7) Dynamic magnetization processes were studied photometrically by the Kerr magnetooptic effect. Barkhausen jumps were observed photometrically during magnetization reversals of a permalloy thin film, and measurements made to determine the integral jump size distribution.

(8) Apparatus was set up for specimen-encircling inductive coil Barkhausen experiments, and preliminary experiments were conducted on cylindrical polycrystalline silicon-iron specimens.

5.2 Plans for Phase III Effort

With the establishment of a solid magnetooptic capability and the promising initial results so far obtained, our magnetooptic effort is now in a position to provide some of the hoped for information needed to clarify certain little-understood aspects of the Barkhausen effect (such as the importance of negative magnetization changes). However, with the magnetooptic work now at a more routine data taking stage, it is anticipated that a considerably larger percentage of time will be devoted to the inductive coil experiments. Preliminary results in this area have defined and clarified a lack of certain instrumentation needed (e.g., a low-noise, broad-band preamplifier) for successful performance of the experiments. Steps have been taken to alleviate this situation. In addition, the recent acquisition of a major instrumentation component (a pulse height analyzer) has given us the capability of doing somewhat more sophisticated experiments than originally intended. Figure 24 shows a sketch of the experimental arrangement to be used in the inductive coil Barkhausen experiments. Use of the pulse height analyzer will allow the Barkhausen pulses to be sorted and stored according to amplitude as the hysteresis loop is traversed. Thus, the distribution of jump sizes along the loop is readily obtained and can be examined under various metallurgical and stressed conditions in polycrystalline specimens.

Availability of the pulse height analyzer also opens doors to more sophisticated magnetooptic experiments. Experiments are planned which make use of the pulse height analyzer in photometric studies of Barkhausen

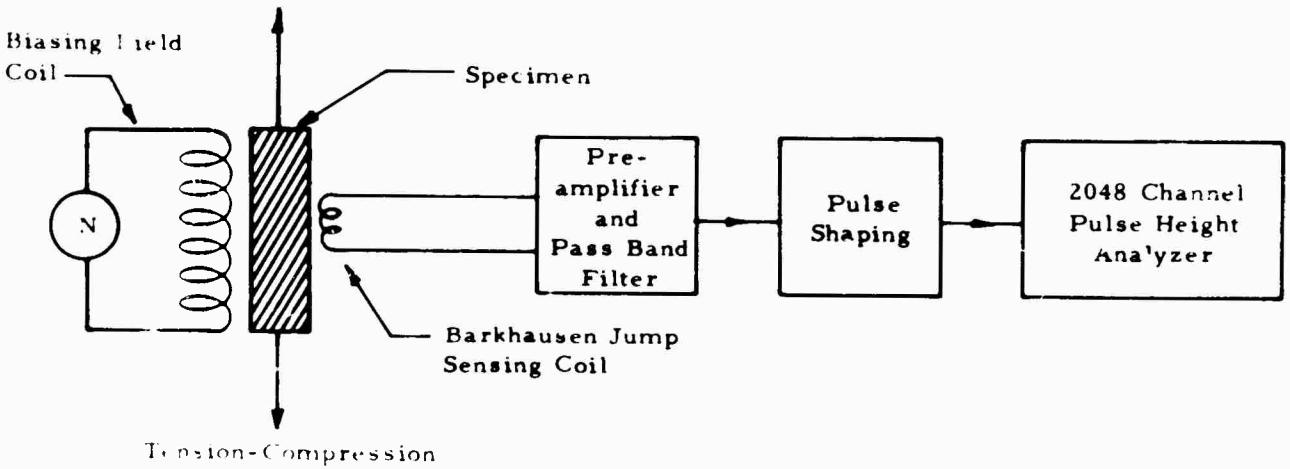

Figure 24. Schematic diagram of experimental arrangement for studying influence of stress upon the distribution of Barkhausen jump sizes as sensed by an induction coil.

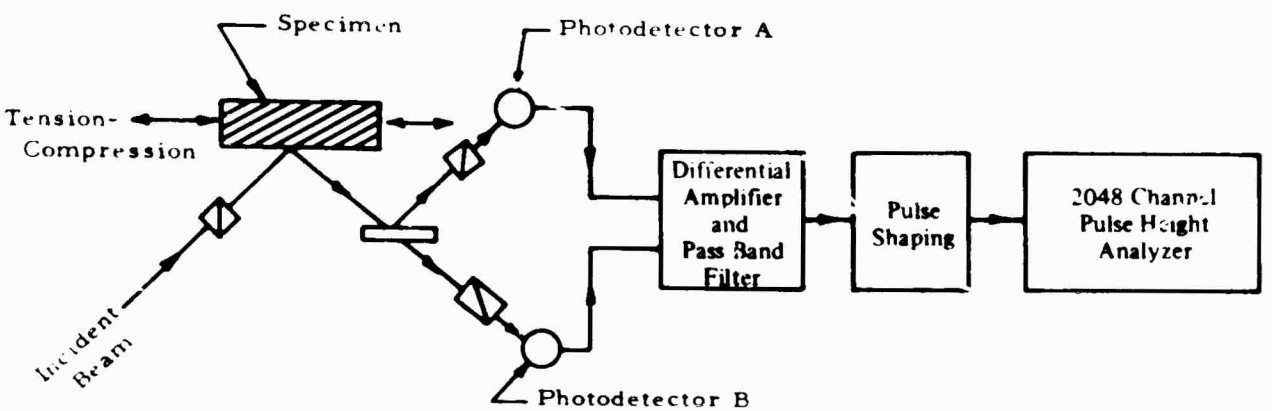

Figure 25. Schematic diagram of experimental arrangement for studying the influence of stress upon the distribution of Barkhausen jump sizes as sensed magnetooptically.

jumps in the silicon-iron single crystal. Figure 25 shows a sketch of the experimental arrangement. The beam reflected off the surface of the specimen is split and passed through separate polarization analyzers and to separate photomultipliers. The analyzers are rotated equal amounts but in opposite directions from the ordinary reflectance plane, and the outputs of the photomultipliers are fed to a differential amplifier. The result is that common mode noise will be cancelled out, whereas the Kerr effect light-intensity changes will be additive. By using high-pass filters or a differentiating system, the abrupt, rapid changes (Barkhausen jumps) show up as pulses which can be sorted and counted by the pulse height analyzer. This provides another method for investigating domain dynamics by the magnetooptic effect and for correlating these observations with Barkhausen signals.

In regard to photographic analysis of domain dynamics, steps have been taken to acquire a recently available stroboscopic burst laser which will enable high-speed cinematographic studies to be made. The laser is capable of firing a burst of pulses at a rate of 6000 pulses/sec with a peak pulse power of about 4 watts. Various measurements and our initial attempts with lower-speed movies have indicated that the conditions available with the burst laser will be sufficient for high-speed cinematographic studies.

Other investigations planned include depth-discrimination experiments using the inductive coil arrangement and magnetooptic studies of polycrystalline specimens.

REFERENCES

1. Bozorth, R. M., Ferromagnetism, D. Van Nostrand Company, Inc., Princeton, New Jersey, 1951, Chapter 13.

2. Zschische, K., "Uber Magnetoelastiche Effekte," J. Phys. 11, 201-214 (1922).

3. Foerster, F. and Stambke, K., "Magnetische Untersuchungen innerer Spannungen, I. Eigenspannungen beim Recken von Nickeldraht," Z. Mettalk. 33, 97 (1941).

4. Leep, R. W., "The Barkhausen Effect and its Application in Nondestructive Testing," Proceedings of the Symposium on Physics and Nondestructive Testing, Dayton, Ohio, 1964, Gordon and Breach, New York, 1967, pp 439-453.

5. Barkhausen, H., "Zwei mit Hilfe der neuen Verstärker entdeckte Erscheinungen," Physik. Z. 20, 400-403 (1919).

6. Donaldson, W. L. and Pasley, R. L., "A New Method of Nondestructive Stress Measurement," Proceedings of the Sixth Symposium on Nondestructive Evaluation of Aerospace and Weapons Systems Components and Materials, Western Periodicals Co., Los Angeles, 1967, pp 563-575.

7. Leep, R. W. and Pasley, R. L., "Method and System for Investigating the Stress Conditioning of Magnetic Materials," U. S. Letters Patent 3,427,872 (1969).

8. Stierstadt, K., "Der Magnetische Barkhausen-Effekt," Springer Tracts in Modern Physics, Vol 40, Springer-Verlag, Berlin, 1966, pp 2-106.

9. Stierstadt, K. and Preuss, E., "Die Temperature-abhangigkeit des magnetischen Barkhausen-Effekts IV, Einfluss des Eigenspannungszustandes," Z. Physik 199, 456-64 (1967), and preceding work cited therein.

10. Matzkanin, G. A., Davidson, D. L., and Gardner, C. G., "Magneto-Optic Study of Domain Dynamics in a Silicon-Iron Single Crystal," Bull. Am. Phys. Soc. 15, 579 (1970).

11. Montalenti, G., "Barkhausen Noise in Ferromagnetic Materials," Z. Angew. Phys. 28, 295-300 (1970), and references cited therein.

12. Kittel, C. and Galt, J. K., "Ferromagnetic Domain Theory," Solid State Physics, Vol 9, Academic Press, New York, 1956, pp 437-564.

13. Lee, E. W., "Magnetostriction and Magnetomechanical Effects," Rep. Prog. Phys. 18, 184-229 (1955).

14. Ibid.

15. Ibid.

16. Kimura, R. and Ohno, K., Sci. Rep. Tohoku Univ., 23, 359 (1934).

17. Kittel, C. and Galt, J. K., op. cit.

18. Ibid., p 479

19. Träuble, H., "Magnetisierung der Ferromagnetika. II. Magnetisierungskurve and magnetische Hysterese ferromagnetische Einkrystalle," Moderne Problem der Metallphysik, Vol 2, Edited by A. Seeger, Springer-Verlag, Berlin, 1966, Chapter 9.

20. Träuble, H., "The Influence of Crystal Defects on Magnetization Processes in Ferromagnetic Single Crystals," Magnetism and Metallurgy, Ed. by Berkowitz, A. E. and Kneller, E., Vol 2, Academic Press, New York, 1969, Chapter XIII, pp 621-687.

21. Fowler, C. A., Jr. and Fryer, E. M., "Magnetic Domains by the Longitudinal Kerr Effect," Phys. Rev. 94, 52 (1954).

22. Stoll, M. P., "The Use of the Magneto-Optical Kerr Effect for the Determination of Magnetization Curves," Phys. Stat. Sol. 22, 163 (1967).

23. Carey, R. and Isaac, E. D., Magnetic Domains and Techniques for Their Observation, Academic Press, New York, 1966.

24. Houze, G. L., Jr., Private communication.

25. Vander Lugt, A., "Signal Detection by Complex Spatial Filtering," IEEE Trans. on Inf. Theory, IT-10, No. 2, 139 (1964).

26. Kranz, J. and Dreschsel, W., Z. Phys. 150, 632 (1958)

27. Houze, G. L., Jr., "Domain Wall Motion in Grain-Oriented Silicon Steel in Cyclic Magnetic Fields," J. Appl. Phys. 38, 1089, (1967).

28. Haller, T. R. and Kramer, J. J., "Observation of Dynamic Domain Size Variation in a Silicon-Iron Alloy," J. Appl. Phys. 41, 1034 (1970).

29. Shilling, J. W., "Grain Boundary Demagnetizing Fields in 3% Si-Fe," J. Appl. Phys. 41, 1165 (1970).

30. Ford, N. C. and Pugh, E. W., "Barkhausen Effect in Nickel-Iron Films," Phys. Rev. 30, 2705 (1959).

31. Stierstadt, K., op. cit.